www.czasopisma.pan.pl PAN www.journals.pan.pl

ARCHIVES of FOUNDRY ENGINEERING

DE GRUYTER OPEN

ISSN (2299-2944)
Volume 15
Issue 1/2015

DOI: 10.1515/afe-2015-0009

Published quarterly as the organ of the Foundry Commission of the Polish Academy of Sciences

41 – 46

# The Reliability of the Results of the Modified Low-cycle Fatigue Test for Cast Iron Evaluated by Metallographic Studies

**M. Maj[a]*, K. Pietrzak[b]**
[a]AGH University of Science and Technology, Faculty of Foundry Engineering,
Department of Foundry Process Engineering, Cracow, Poland
[b]Motor Transport Institute, 03-301 Warsaw, Poland
*Corresponding author. E-mail address: mmaj@agh.edu.pl

Received 04.07.2014; accepted in revised form 22.07.2014

## Abstract

This study discloses the characteristic features of the modified low-cycle fatigue test used for the determination of the mechanical properties of two types of cast iron, i.e. EN-GJL-250 and EN-GJS-600-3. For selected materials, metallographic studies were also conducted in the range of light microscopy and scanning microscopy.

**Keywords**: Cast iron with lamellar graphite, Cast iron with spheroidal graphite, Low-cycle fatigue test, Mechanical properties

## 1. Low-cycle fatigue test and modified low-cycle fatigue test (LCF vs MLCF)

The analysis of mechanical properties in a range of alternate low-cycle loads in Manson, Coffin and Morrow's approach [2, 3, 4, 5, 6] covered also by a Polish standard [7] and known as LCF (Low Cycle Fatigue) test consists in tests carried out under the conditions of symmetric loads. The applied load causes alternate tension and compression of the specimen within the range of „hypercritical" stresses, i.e. above the fatigue limit, starting usually with the stress amplitude causing permanent strain of minimum 0,2 %. Under such conditions, it becomes possible to reduce the number of cycles to specimen failure, while the results of a test performed on one specimen are expressed by one point on the low-cycle fatigue curve (Fig. 1). Hence it logically follows that the results are the more precise, the larger is the number of the specimens used in tests.

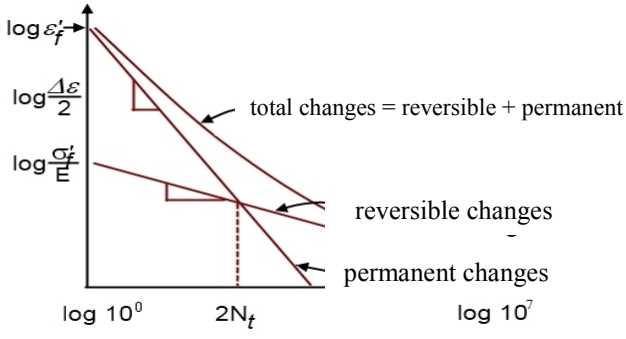


Fig. 1. A fatigue life curve in logarithmic coordinates [3]

Practical application of the LCF test is limited to materials characterised by good plastic properties, since the whole measuring range is substantially lying well above the yield point [3, 4]. As claimed by a respective standard [7], the test consists in subjecting the specimens to uniaxial changing loads (tension – compression) until failure occurs and in recording during the test the number of cycles and plotting the stress-strain (force-displacement) curve in the form of a hysteresis loop. The test is conducted through control of either stress (force referred to the initial specimen cross-section), or deformation (of specimen measurement base), or displacement (of loading system).

The determination by this method of the critical number of cycles for several values of the amplitude enables also the determination of various other criteria useful in the evaluation of materials, the upper strain limit included.

According to the above mentioned researchers, the following equations can be written down:

$$\sigma_a = K' (\varepsilon_p)^{n'} \quad (1)$$

$$\sigma_a = \sigma'_f (2N_f)^b \quad (2)$$

$$\varepsilon_p = \varepsilon'_f (2N_f)^c \quad (3)$$

where:

- $\sigma_a$ – the stress cycle amplitude,
- $\sigma'_f$ – the, so called, fatigue life coefficient roughly equal to the tensile strength $R_m$,
- $\varepsilon_f$ – the true permanent strain induced by stress $\sigma_f$
- $2N_f$ – the number of loading cycles to specimen failure,
- $\varepsilon_p$ – the true permanent strain induced by $2N_f$ loading cycles, where: $\varepsilon_p = \ln(1 + \varepsilon_k)$, and where $\varepsilon_k = \Delta l_{trwałe} / l_0$
- $K'$ – the cyclic strength coefficient,
- $n'$ – the strain-hardening exponent for alternate cyclic loads,
- c – the fatigue ductility exponent,
- b – the Basquin's exponent.

Assuming constant (over the whole stress range up to fatigue limit) value of the modulus of elasticity E, the following equation can be written down for the elastic strain $\varepsilon_e$:

$$\varepsilon_e = \sigma_f / E^* (2N_f)^b \quad (4)$$

Assuming $2N_f$ equal to a minimum number of the loading cycles that the material is expected to endure under the effect of changing stresses of an amplitude $\sigma_a$ equal to a fatigue strength limit (the „reference" number of cycles), the following equation can be written down to allow for total strain ($\varepsilon_c$) after this number of cycles and after any arbitrary lower number of cycles:

$$\varepsilon_c = \varepsilon_e + \varepsilon_f = \varepsilon_e = \sigma_f / E^* (2N_f)^b + \varepsilon'_f (2N_f)^c \quad (5)$$

It is worth noting that calculating the above mentioned parameters in a low-cycle fatigue test requires the use of 6 to 10 specimens, which raises problems in the case of materials structurally inhomogeneous. In its modified form (MLCF) [3, 4] this method enables the same parameters to be determined on one specimen only, as discussed extensively in other studies [3, 4, 7, 10].

The fatigue strength $Z_{go}$, necessary for the computation of test parameters, is determined from a test curve plotted for different material families, starting with pure metals and ending in ferrous and non-ferrous metal alloys [3, 4].

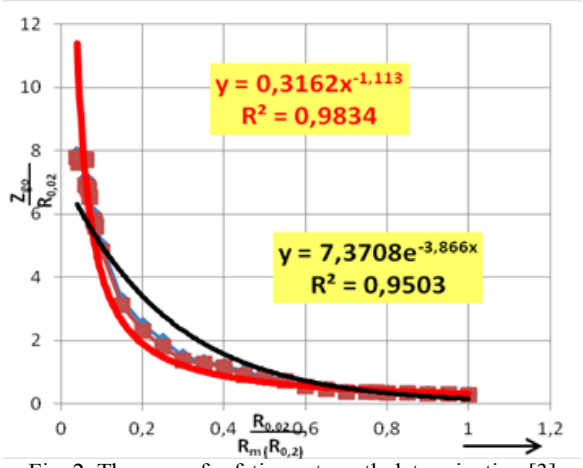


Fig. 2. The curve for fatigue strength determination [3]

## 2. Test material and results

In this study, fatigue tests were carried out according to the MLCF procedure on samples of the two types of cast iron, i.e. EN-GJS-600-3 and EN-GJL-250. The results of the tests done in accordance with the MLCF methodology are compared in Tables 1 and 2 for the EN-GJS-600-3 cast iron and EN-GJL-250 cast iron, respectively, Additionally, metallographic studies were performed using light microscopy and scanning microscopy. Quantitative research was conducted on computer image analyser coupled on-line with a light microscope. In view of the qualitatively stable microstructure of the cast iron metal matrix, quantitative studies of the microstructure of cast iron with spheroidal and lamellar graphite were limited to the sole graphite, basing on the assumption that possible variations in the volume content of graphite and its morphological features can significantly affect the achieved level of mechanical properties. In this case, the measurements were taken at 500x magnification to account also for the graphite precipitates of smaller size. Prior to systematic studies, the relevance of a fixed number of the examined measurement fields, which in the case under discussion amounted to 100, was verified by random experiments. More than 100 fields did not change significantly the results obtained and unnecessarily prolonged the time required for a full measurement cycle. Based on the results of the measurements taken, geometrical parameters were specified for the spheroidal graphite in ductile iron and for the lamellar graphite in grey cast iron:

- $A_A = V_V$ [%] - the volume fraction of pores/ graphite,
- $N_{L\parallel}$ and $N_{L\perp}$ - estimators of the relative area of pores/graphite measured in two mutually perpendicular directions,

$\Omega$- coefficient of microstructural anisotropy,
$l_{II}$ and $l_{\perp}$ - average chords of pores/graphite measured in two mutually perpendicular directions,
$F_{śr}$- average Feret diameter of pores/graphite

Table 1.
The mechanical properties of EN-GJS-600-3 cast iron determined on the basis of fatigue tests performed in accordance with the MLCF methodology

| No. | E [MPa] | $R_m$ [MPa] | $R_{0,02}$ [MPa] | $R_{0,2}$ [MPa] | $Z_{go}$ [MPa] | $R_a$ [MPa] |
|---|---|---|---|---|---|---|
| 1 | 198 629 | 569,5 | 339,4 | 478,8 | 188,5 | 533,6 |
| 2 | 194 857 | 556,7 | 340,7 | 469,3 | 186,0 | 533,0 |
| 3 | 179 029 | 532,8 | 342,7 | 487,3 | 191,4 | 492,3 |
| 4 | 198 857 | 600,8 | 347,9 | 485,9 | 191,8 | 573,1 |
| 5 | 193 006 | 492,7 | 308,2 | 483,5 | 182,8 | 491,9 |
| 6 | 180 362 | 532,7 | 343,5 | 488,1 | 191,8 | 492,4 |
| 7 | 180 215 | 492,0 | 430,9 | 446,4 | 181,8 | 451,8 |
| 8 | 190 315 | 573,2 | 411,1 | 489,1 | 226,1 | 532,4 |

| No. | b | c | n' | K' [MPa] | $\varepsilon_{max} \cdot 10^6$ |
|---|---|---|---|---|---|
| 1 | -0,0960 | -0,4456 | 0,1060 | 933,9 | 1069 |
| 2 | -0,0953 | -0,5349 | 0,0907 | 848,9 | 899 |
| 3 | -0,0889 | -0,3426 | 0,1708 | 1461,9 | 1156 |
| 4 | -0,0996 | -0,5249 | 0,1039 | 938,7 | 1001 |
| 5 | -0,0861 | -0,3635 | 0,1497 | 1267,2 | 1005 |
| 6 | -0,0887 | -0,3326 | 0,1547 | 1345,6 | 1116 |
| 7 | -0,0865 | -0,3603 | 0,1597 | 1318,2 | 0977 |
| 8 | -0,0808 | -0,5692 | 0,0917 | 872,9 | 1141 |

Figures 3-14 show images of microstructure in selected samples of EN-GJS-600-3 ductile iron revealed by light microscopy.

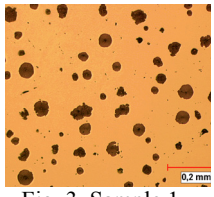
Fig. 3. Sample 1 Graphite in EN-GJS-600-3 cast iron, 100x, ordinary light

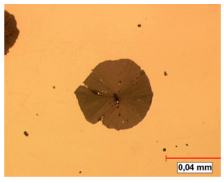
Fig. 4. Sample 1 Graphite in EN-GJS-600-3 cast iron, 500x, ordinary light

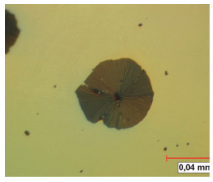
Fig. 5. Sample 3 Graphite in EN-GJS-600-3 cast iron, 500x, phase contrast

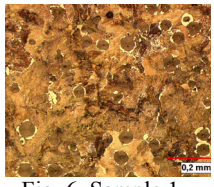
Fig. 6. Sample 1 Metal matrix in EN-GJS-600-3 cast iron, 100x, ordinary light

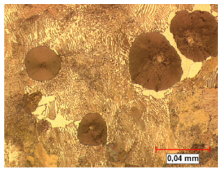
Fig. 7. Sample 1 Metal matrix in EN-GJS-600-3 cast iron, 500x, ordinary light

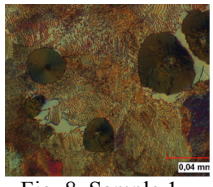
Fig. 8. Sample 1 Metal matrix in EN-GJS-600-3 cast iron, 500x, phase contrast

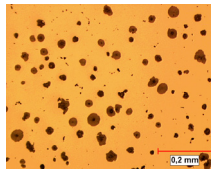
Fig. 9. Sample 8 Graphite in EN-GJS-600-3 cast iron, 100x, ordinary light

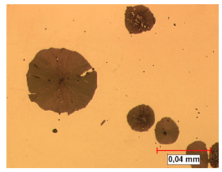
Fig. 10. Sample 8 Graphite in EN-GJS-600-3 cast iron, 500x, ordinary light

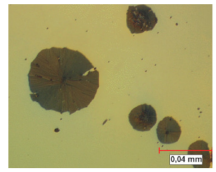
Fig. 11. Sample 8 Graphite in EN-GJS-600-3 cast iron, 500x, phase contrast

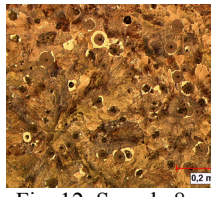
Fig. 12. Sample 8 Metal matrix in EN-GJS-600-3 cast iron, 100x, ordinary light

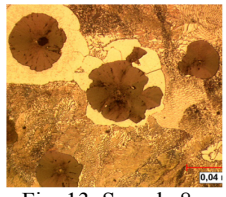
Fig. 13. Sample 8 Metal matrix in EN-GJS-600-3 cast iron, 500x, ordinary light

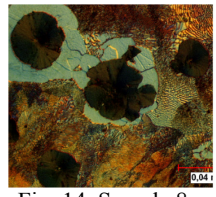
Fig. 14. Sample 8 Metal matrix in EN-GJS-600-3 cast iron, 500x, phase contrast

Fractures of samples obtained in fatigue test performed by MLCF and revealed by SEM (Figs. 15-26) show qualitatively similar character and can be classified as brittle. At higher magnifications, smooth fragments of the fracture forming cleavage planes are observed; cracks and tears are also visible.

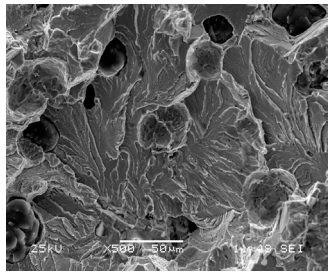
Fig. 15. EN-GJS-600-3 cast iron, Sample 1, 500x, SEM

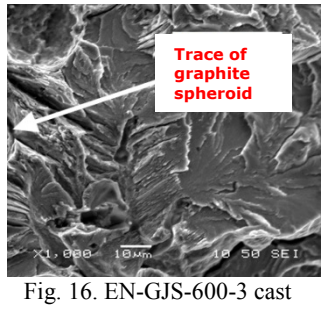

Fig. 16. EN-GJS-600-3 cast iron, Sample 1, 1000x, SEM

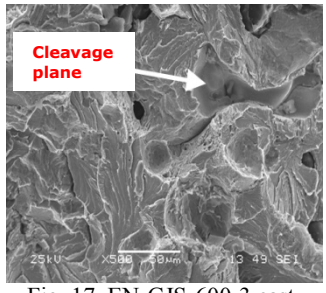

Fig. 17. EN-GJS-600-3 cast iron, Sample 8, 500x, SEM

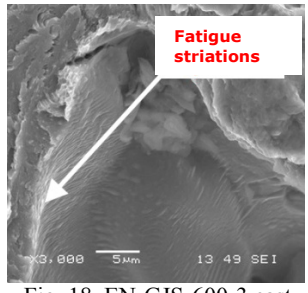

Fig. 18. EN-GJS-600-3 cast iron, Sample 8, 3000x,SEM

Table 2.
The mechanical properties of EN-GJL-250 cast iron determined on the basis of fatigue tests performed in accordance with the MLCF methodology

| No. | E [MPa] | $R_m$ [MPa] | $R_{0,02}$ [MPa] | $R_{0,2}$ [MPa] | $Z_{go}$ [MPa] | $R_a$ [MPa] |
|---|---|---|---|---|---|---|
| 1 | 128 406 | 193,1 | 82,2 | 143,3 | 51,3 | 175,1 |
| 2 | 126 972 | 200,5 | 106,0 | 156,3 | 60,7 | 173,3 |
| 3 | 125 215 | 199,4 | 80,5 | 142,5 | 50,7 | 175,5 |
| 4 | 125 789 | 196,5 | 75,2 | 157,0 | 54,9 | 173,8 |
| 5 | 124 711 | 199,8 | 62,8 | 158,9 | 55,3 | 181,9 |
| 6 | 126 576 | 192,9 | 61,8 | 153,3 | 55,4 | 182,4 |
| 7 | 124 252 | 195,5 | 90,2 | 149,5 | 53,2 | 171,8 |

| No. | b | c | n' | K' [MPa] | $\varepsilon_{max} \cdot 10^6$ |
|---|---|---|---|---|---|
| 1 | -0,1151 | -0,4816 | 0,2019 | 599,1 | 432 |
| 2 | -0,1038 | -0,3846 | 0,2035 | 603,8 | 746 |
| 3 | -0,1189 | -0,6204 | 0,1909 | 550,3 | 372 |
| 4 | -0,1108 | -0,3119 | 0,2103 | 642,3 | 907 |
| 5 | -0,1085 | -0,3686 | 0,1906 | 535,3 | 786 |
| 6 | -0,1099 | -0,3845 | 0,1899 | 639,2 | 450 |
| 7 | -0,1135 | -0,3699 | 0,2011 | 585,4 | 399 |
| 8 | -0,1146 | -0,4511 | 0,1954 | 299,2 | 520 |

Figures 19-30 show images of microstructure in samples of EN-GJL-250 cast iron revealed by light microscopy, while Figures 31-36 show images of fractures produced in these samples by the MLCF fatigue test and revealed by SEM.

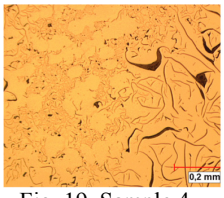
Fig. 19. Sample 4 Lamellar graphite in EN-GJL-250 cast iron, 100x, ordinary light

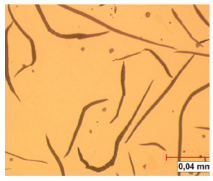
Fig. 20. Sample 4 Lamellar graphite in EN-GJL-250 cast iron, 500x, ordinary light

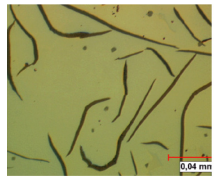
Fig. 21. Sample 4 Lamellar graphite in EN-GJL-250 cast iron, 500x, phase contrast

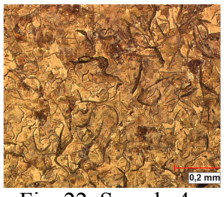
Fig. 22. Sample 4 Metal matrix in EN-GJL-250 cast iron, 100x, ordinary light

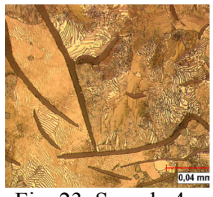
Fig. 23. Sample 4 Metal matrix in EN-GJL-250 cast iron, 500x, ordinary light

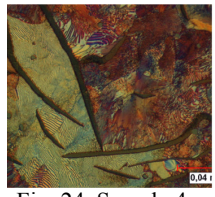
Fig. 24. Sample 4 Metal matrix in EN-GJL-250 cast iron, 500x, phase contrast

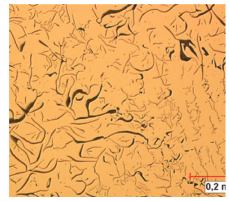
Fig. 25. Sample 5 Lamellar graphite in EN-GJL-250 cast iron, 100x, ordinary light

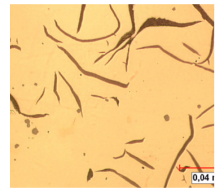
Fig. 26. Sample 5 Lamellar graphite in EN-GJL-250 cast iron, 500x, ordinary light

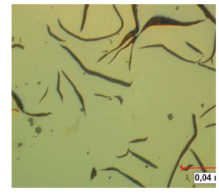
Fig. 27. Sample 5 Lamellar graphite in EN-GJL-250 cast iron, 500x, phase contrast

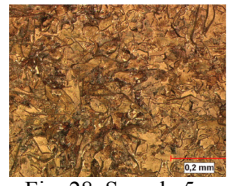
Fig. 28. Sample 5 Metal matrix in EN-GJL-250 cast iron, 100x, ordinary light

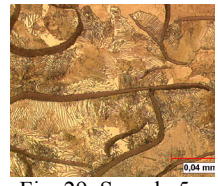
Fig. 29. Sample 5 Metal matrix in EN-GJL-250 cast iron, 500x, ordinary light

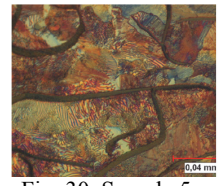
Fig. 30. Sample 5 Metal matrix in EN-GJL-250 grey cast iron, 500x, phase contrast

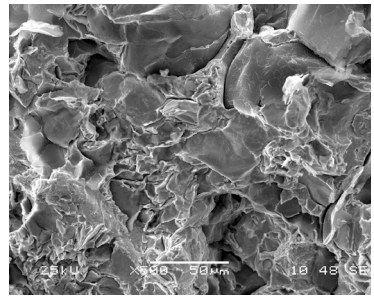
Fig. 31. EN-GJL-250 cast iron Sample 3, x500, SEM

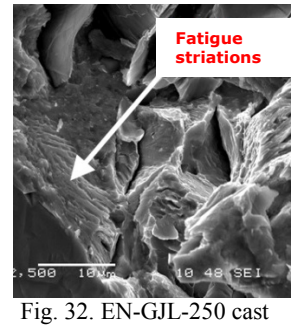

Fig. 32. EN-GJL-250 cast iron, Sample 3, x2500, SEM

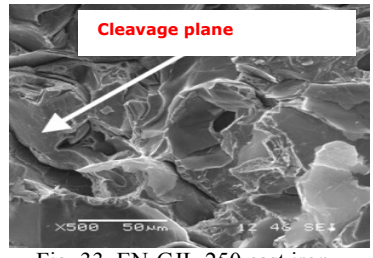

Fig. 33. EN-GJL-250 cast iron Sample 4, x500, SEM

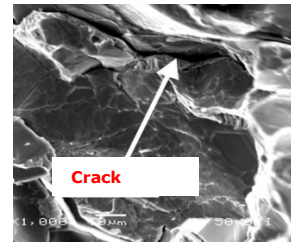

Fig. 34. EN-GJL-250 cast iron, Sample 4, x1000, SEM

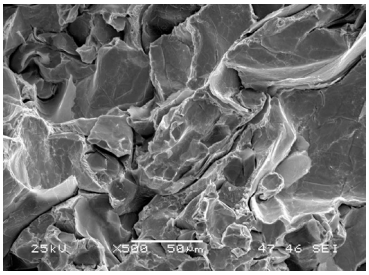


Fig. 35. EN-GJL-250 cast iron Sample 5, x500, SEM

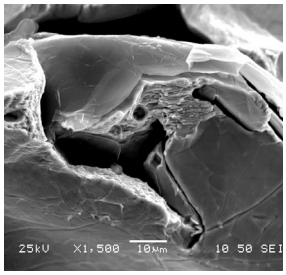


Fig. 36. EN-GJL-250 cast iron, Sample 5, x1000, SEM

In this study, the results of quantitative metallographic analysis are presented only for the EN-GJS-600-3 ductile iron and are compared in Table 3. Photographs of microstructure showed earlier in the text in Figure 37 illustrate true (black and white) images of graphite precipitates in the examined cast iron and binary images prepared for quantitative analysis where graphite is distinguished by yellow colour. The results of quantitative measurements are compared in Table 3. They prove that all the measured geometrical parameters of spheroidal graphite show nearly no variations – the fact which is also reflected in the resulting stable mechanical properties tested by MLCF.

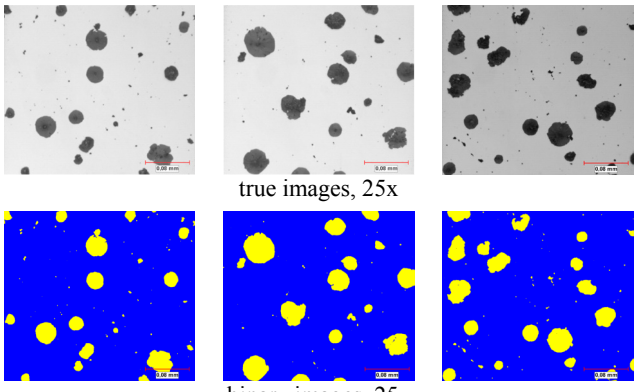

true images, 25x

binary images, 25x

**Sample 1** **Sample 2** **Sample 3**

Fig. 37. Images of microstructure (EN-GJS-600-3 cast iron) – true and binary images

Table 3.
Geometrical parameters of graphite in EN-GJS-600-3 cast iron

| Material | Sample No. | Statistical quantity | Geometrical parameters of graphite | | | | | | | |
|---|---|---|---|---|---|---|---|---|---|---|
| | | | $\overline{A}_A$ | $\overline{N}_{LII}$ | $\overline{N}_{L\perp}$ | $\overline{N}_A$ | $\overline{\Omega}$ | $\overline{F}_{śr}$ | $\overline{l}_{II}$ | $\overline{l}_{\perp}$ |
| | | | [%] | [1/mm] | [1/mm] | [1/mm$^2$] | - | [mm] | [mm] | [mm] |
| EN-GJS-600-3 cast iron | 1 | Mean | 9,81 | 65,9 | 64,6 | 682 | 1,02 | 0,009 | 0,015 | 0,016 |
| | | Standard deviation | 1,70 | 7,1 | 6,9 | 89 | 0,04 | 0,012 | 0,002 | 0,002 |
| | 2 | Mean | 10,03 | 61,1 | 61,4 | 687 | 1,01 | 0,009 | 0,016 | 0,017 |
| | | Standard deviation | 1,95 | 8,8 | 8,3 | 86 | 0,05 | 0,012 | 0,002 | 0,002 |
| | 3 | Mean | 10,01 | 68,1 | 66,6 | 829 | 1,02 | 0,008 | 0,015 | 0,015 |
| | | Standard deviation | 1,90 | 10,2 | 10,0 | 249 | 0,04 | 0,011 | 0,002 | 0,002 |
| | **mean** | **Mean** | **9,95** | **65,0** | **64,2** | **733** | **1,02** | **0,009** | **0,015** | **0,042** |
| | | **Standard deviation** | **0,09** | **2,6** | **1,9** | **64** | **0,004** | **0,0004** | **0,004** | **0,034** |

Analysing the results of mechanical tests performed by MLCF on the EN-GJS-300 and EN GJL-250 cast irons, the main attention deserve the parameters *b* and *c* which in the low-cycle fatigue test describe the examined material in terms of its mechanical and plastic properties, since *b* is the fatigue strength exponent and *c* is the fatigue ductility exponent, and as such they are both extremely sensitive verifiers of these properties. Additionally, these are the exponents that have a direct impact on the magnitude of the maximum total strain $\varepsilon_{max}$ (equation 5) which, in turn, determines the fatigue life of a material or structure. According to the literature data [2], both these parameters should be comprised within the range of the following values:

**b: from -0.05 to -0.15; c: from -0.5 to - 0.7**

The fatigue strength exponent decreases with the decreasing strength (its absolute value is increasing), while the fatigue ductility exponent decreases with the increasing plastic properties of the material (its absolute value is increasing).

As regards the EN-GJS-600-3 cast iron (Table 1), the parameter *b* is roughly in the middle range of occurrence, if the arithmetic mean value (b = -0.090225) is taken into account. On the other hand, examining all samples of this material in sequence, no clear relationship has been observed to occur between the drop in endurance limit and the increase in an absolute value of the exponent *b*. The explanation can be sought in the fact that variations in these values are very small and as such may not be reflected in the mutual interdependencies.

As regards the fatigue ductility exponent, its average value is slightly below the lower range of occurrence (c = -0.4342). In contrast, the average value of the maximum total allowable strain ($\varepsilon_{max}$) is for this material $\varepsilon_{max} \cdot 10^6 = 1045$.

Examining the results of the mechanical tests of the EN-GJL-250 cast iron (Table 2), it can be seen that the values of $R_m$ are underrated, which can indicate the manner of sample preparation (casting). The fatigue strength exponent *b* is in the upper range of occurrence (mean *b* = -0.1118) and comparing its value with the average value of the parameter *b* for the EN-GJS-600-3 cast iron (*b* = -0.090225), a relationship with the value of $R_m$, can be observed, i.e. the lower is the $R_m$ value, the lower is the value of the exponent *b* (the higher is its absolute value). As regards the fatigue ductility exponent, its value is slightly below the lower range of occurrence (mean *c* = 0.4216). In contrast, for the EN-GJL-250 cast iron, the average value of the maximum total allowable strain ($\varepsilon_{max}$) is $\varepsilon_{max} \cdot 10^6 = 576$.

## 3. Conclusions

1. The modified method of fatigue strength testing (MLCF) allows determining on one sample only the static mechanical properties ($R_m$, $R_{0,02;}R_{0,2;}$ estimated value of $Z_{go}$) and properties characteristic of the material fatigue behaviour (b, c, $\varepsilon_{max}$).
2. The results of quantitative measurements taken by the methods of quantitative metallography on graphite spheroids in ductile iron exhibit virtually no variations, the fact which is further reflected in the stable mechanical properties of this cast iron checked by the MLCF test. Thus, the usefulness of the MLCF test as an effective tool in studies of the mechanical properties based on data obtained on a single sample was confirmed.
3. 3 The results obtained clearly demonstrate the satisfactory sensitivity of the MLCF method to any differences in the microstructure.

## References

[1] *Cast iron. Inoculation. The technology of graphite shape control*, ISO/TS 16949 ISO 14001, www.foundry.elkem.com [2 July 2011].
[2] Kocańda, S., Kocańda, A. (1989). *Low cycle fatigue strength of metals*, PWN – W-wa. (in Polish).
[3] Maj, M. (1984). *The criteria for the operational strength of cast iron, based on the mechanical properties of materials*. Doctoral dissertation. Kraków. (in Polish).
[4] Karamara, A. (1980). *Material tests of selected species in the range of low alloy steel niskocyklicznych variable loads*. Kraków . Z-5216/79. (in Polish).
[5] Kocańda, S. (1978). *Metal fatigue destruction*, WNT Warszawa. (in Polish).
[6] Socie, D.F., Mitchell, M.R. & Caulfield, E.M. (1977). Fundamentals of Modern Fatigue Analysis, A Report of the Fracture Control Program, *College of Engineering*. University of Illinois Urbana, Illinois 61801, April, 1977. Revised January 1978.
[7] PN-84/H-04334: Low-cycle fatigue tests of metals. (in Polish)
[8] Maj, M., *Self nr 10.10.170.34: Optimization of the low cycle fatigue test test. No Publisher.* (in Polish)
[9] Karamara, A. (1971). Determining the strength of shape castings based on the border of accommodation. *Metalurgia* 17 Prace Komisji Metalurgiczno-Odlewniczej. PAN – Oddział w Krakowie..
[10] Maj, M. (2005). The research project 4T8B00625 *The use of a modified, low cycle fatigue test to determine the mechanical properties of ADI at room temperature and elevated*, Kraków. (in Polish).
[11] Maj, M. (2012). *Fatigue selected alloys.* Ed. Archives of Foundry Engineering, Katowice-Gliwice.